

A Fully-Integrated Flexible Photonic Platform for Chip-to-Chip Optical Interconnects

Lan Li, *Student Member, IEEE*, Yi Zou, Hongtao Lin, Juejun Hu, *Member, IEEE*, Xiaochen Sun, Ning-Ning Feng, Sylvain Danto, Kathleen Richardson, Tian Gu, *Member, IEEE*, and Michael Haney, *Member, IEEE*

Abstract—We analyze a chip-to-chip optical interconnect platform based on our recently developed flexible substrate integration technology. We show that the architecture achieves high bandwidth density (100 Tbs/cm²), and does not require optical alignment during packaging. These advantages make the flexible photonics platform a promising solution for chip-to-chip optical interconnects. We further report initial experimental characterizations of the flexible photonics platform fabricated using thermal nanoimprint patterning of glass waveguides and III–V die bonding.

Index Terms—Data communications, energy per bit, optical interconnects, optical waveguides.

I. INTRODUCTION

THERE is an increasing need for high performance computing (HPC) that exploits low-energy-per-bit transmission and high data bandwidth of interconnect networks between the computational cores, memories, and external cache. According to the ITRS Roadmap, the total on/off chip data I/O is projected to reach 100 Tb/s at the 9 nm node, far exceeding the capacity that can be possibly reached using current copper wiring technology. Optical interconnects have been intensively investigated as a potential solution to resolve this “interconnect bottleneck.” The solutions typically involve on-chip edge-view active components coupled to optical fiber bundles [1], [2] or surface mount VCSELs and detectors vertically integrated with on-board multi-mode waveguides [3], [4]. Both approaches, however, are not scalable to high bandwidth density due to chip geometry constraints. For example, given an edge-coupled fiber pitch of 100 μm and a single channel bandwidth of 10 Gb/s, the aggregate off-chip bandwidth is limited to 10 Tb/s for a 2.5 cm by 2.5 cm chip (assuming all four chip edges are used

Manuscript received July 1, 2013; revised September 2, 2013; accepted October 5, 2013. Date of publication October 9, 2013; date of current version November 27, 2013. This work was supported in part by the Delaware NASA EPSCoR RID Seed Grant Program. L. Li and Y. Zou contributed equally to this work.

L. Li, Y. Zou, H. Lin, and J. Hu are with the Department of Materials Science & Engineering, University of Delaware, Newark, DE 19716 USA (e-mail: lanli@udel.edu; zouyi@udel.edu; hometown@udel.edu; hujuejun@udel.edu).

X. Sun and N.-N. Feng are with the LaXense Inc., Walnut, CA 91789 USA (e-mail: xchsun@gmail.com; fengn00@gmail.com).

S. Danto and K. Richardson are with the College of Optics & Photonics, University of Central Florida, Orlando, FL 32816 USA (e-mail: sylvain.danto1@gmail.com; kcr@creol.ucf.edu).

T. Gu and M. Haney are with the Electrical & Computer Engineering Department, University of Delaware, Newark, DE 19716 USA (e-mail: tgu@udel.edu; michaelwhaney@gmail.com).

Color versions of one or more of the figures in this paper are available online at <http://ieeexplore.ieee.org>.

Digital Object Identifier 10.1109/JLT.2013.2285382

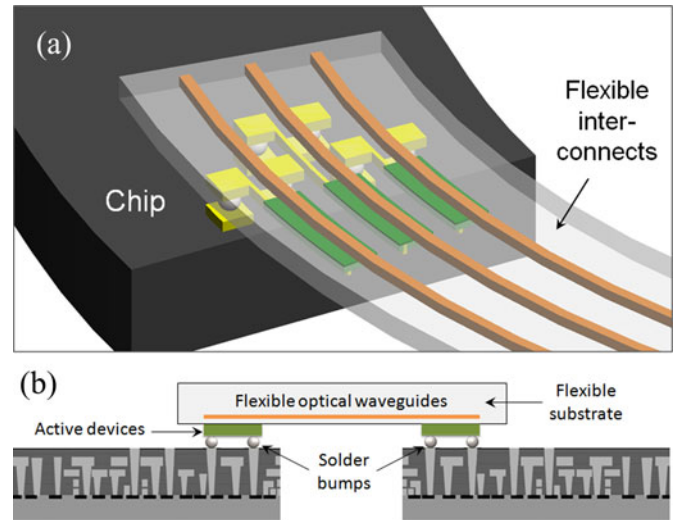


Fig. 1. The fully-integrated flexible optical interconnect design: (a) schematic tilted view of a flexible optical link bonded to a chip; (b) cross-sectional structure of the optical link.

for coupling with the waveguides and no wavelength division multiplexing is implemented). Wavelength division multiplexing (WDM) can alleviate the bandwidth density bottleneck; however, WDM (in particular dense WDM) dramatically complicates system design and consumes significantly more power due to the needs for thermal tuning and temperature stabilization. New solutions scalable to the 10 Tb/s regime and beyond is thus mandated to resolve the chip-to-chip interconnect challenge, and several innovative interconnect designs are currently being investigated, such as multi-core fiber interconnects [5], optical printed circuit boards [6], [7], silicon photonics [8], [9], and hybrid approaches [10]–[15]. In this paper, we propose and analyze a new chip-to-chip interconnect scheme based on a flexible photonics platform we developed. We show that the design offers scalable high bandwidth density and potentially enables a simplified packaging solution without involving optical alignment.

II. FULLY-INTEGRATED FLEXIBLE OPTICAL INTERCONNECT: A SYSTEM-LEVEL ANALYSIS

Fig. 1(a) schematically illustrates the proposed interconnect design. The interconnect architecture builds on a flexible planar photonic link, which consists of an array of single-mode glass optical waveguides on a common flexible substrate as well as active optoelectronic components (lasers and detectors) bonded onto the flexible substrate and optically coupled to the

waveguides. The active devices based on an alignment-free die-to-wafer bonding process [16]–[18] and are directly coupled to the waveguides. Two ends of the flexible link is flip-chip bonded and electrically connected to chips through solder bumps and on-chip metal vias, which also serve as effective heat conduction channels between the active devices and the chip. Our thermal diffusion simulations indicate a temperature rise of $<20^\circ\text{C}$ (relative to the chip) at the proposed integration density, which is acceptable for active device operation. The flexible link interconnects present several unique advantages for chip packaging:

- 1) given the limited positioning accuracy of current “pick-and-place” chip placement technologies ($\sim 10\ \mu\text{m}$), mechanical flexibility of the link is essential to accommodate misalignment between chips surface-mounted on carriers or on a printed circuit board;
- 2) since the optical link only interfaces with the chips electronically, no optical alignment is required during packaging. In this sense, the flexible optical interconnects may be viewed as the planar counterpart of active optical cables, although their planar design offers much higher bandwidth density;
- 3) the low-profile flexible link (total thickness can be scaled down to below $25\ \mu\text{m}$) is compatible with integration on flip-chip bonded chips.

In addition to these packaging benefits, the flexible interconnect platform also offers large bandwidth density and low power consumption. In the configuration shown in Fig. 1, the interconnect bandwidth density is only limited by the physical sizes of on-chip contact pads and solder bumps, and not by the limited optical alignment accuracy or optical coupler size. Unlike edge coupling to optical waveguides (the “1-D” approach), on-chip contact pads can be arranged to form 2-D arrays, which dramatically increases the bandwidth density scalability. In addition, since there is no optical alignment requirement during packaging, our approach adopts single mode, high-index-contrast glass waveguides for optical interconnects, which also contributes to high-density integration not limited by the large multi-mode waveguide or fiber pitch. Assuming a bonding pad pitch of $100\ \mu\text{m}$ which is readily achievable using flip-chip bonding [22], the on-chip real estate needed for one transceiver-receiver optical link is $0.02\ \text{mm}^2$, corresponding to an simplex areal bandwidth density of $100\ \text{Tbs/cm}^2$ provided that each link channel operates at $10\ \text{Gb/s}$. The bandwidth scalability benefit of our approach is illustrated in Table I, where we compare the possibly attainable aggregate bandwidths of several interconnect solutions. In the comparison, we assume the same $10\ \text{Gb/s}$ single channel data rate, $2.5\ \text{cm} \times 2.5\ \text{cm}$ chip size, and all four chip edges are used for interconnects. Based on the $100\ \text{Tbs/cm}^2$ band width density number, the chip-to-chip interconnects will occupy a $1\ \text{mm}$ wide patch on the entire chip periphery. It is apparent that the bandwidth density of traditional 1-D edge-coupling optical interconnect schemes are limited by the physical size of the chip to $<20\ \text{Tb/s}$, while our approach enables off-chip I/O bandwidth scalable to $100\ \text{Tb/s}$ which sufficiently accommodates the interconnect bandwidth need at $9\ \text{nm}$ CMOS node. Notably, the areal interconnect density is still ultimately limited by the waveguide pitch as the 2-D

TABLE I
BANDWIDTH SCALABILITY OF OUR FLEXIBLE OPTICAL INTERCONNECT PLATFORM AS COMPARED TO OTHER COMPETING OPTICAL INTERCONNECT TECHNOLOGIES

Technology	Waveguide pitch (μm)	Total I/O channel #	Aggregate data rate (Tb/s)
Flexible optical interconnect	10	5,000	100
Polymer optical fiber ribbons [2]	250	200	4
Multi-mode on-board waveguides [3, 19]	62.5	800	16
Multi-mode off-board waveguides [20, 21]	200	250	5

TABLE II
OPTICAL LOSS BUDGET (IN dB) OF THE FLEXIBLE INTERCONNECT PLATFORM (PROJECTED) AND TYPICAL VCSEL-BASED MULTI-MODE OPTICAL LINKS

Loss mechanisms	Flexible single-mode photonics	VCSEL-based multi-mode optics
Laser-to-waveguide coupling loss	0	1.1 [23]
Modulator insertion loss	1 [24]	0
Waveguide-to-PD coupling loss	0.5 [25]	1.1 [23]
Waveguide propagation loss	4 [26]	0
Extinction ratio penalty	3	3
Margin	4	4
Total	12.5	9.2

interconnect waveguide structure collapses into a 1-D structure at the chip edge. Our simulations indicate that a small waveguide spacing of $6\ \mu\text{m}$ is sufficient to guarantee $<-40\ \text{dB}$ inter-channel cross-talk in a $40\ \text{cm}$ long optical link given the relatively high index contrast of the flexible optical waveguides. Thus our single-mode design allows small waveguide pitch ($<10\ \mu\text{m}$) compatible with high-density 2-D integration.

Next we show that the flexible interconnect platform promises low energy consumption comparable or even superior to that of high-performance VCSEL-based links. Table II compares the estimated optical loss budget of our technology with that of VCSEL-based multi-mode optics which include the three current technology platforms listed in Table I. The numbers listed in the table are based on values previously reported in literature. Since the evanescent lasers used in the flexible photonic links are waveguide coupled, the laser-waveguide coupling loss vanishes as it becomes part of the laser efficiency. These numbers indicate comparable optical loss for both types of interconnect links and support a low power laser source owing to high sensitivity of modern receivers (typically better than $-18\ \text{dBm}$ at $10\ \text{Gb/s}$ [27]). In our case, the required output optical power of a continuous-wave (CW) bonded laser is $-5.5\ \text{dBm}$ so laser power consumption is currently dominated by relatively large

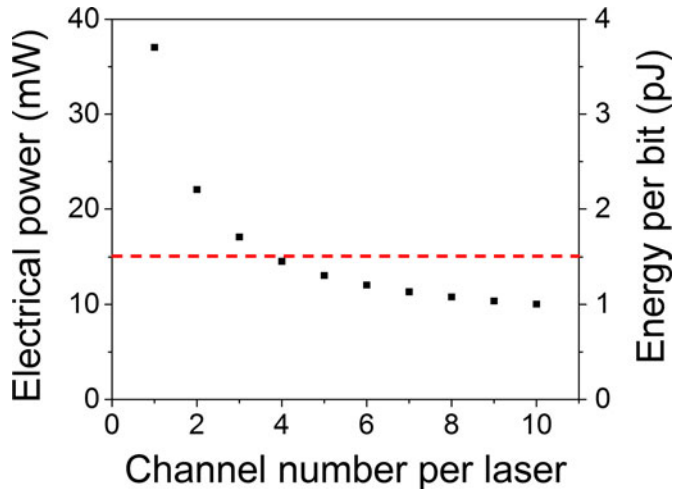


Fig. 2. Single channel electrical power consumption of the flexible optical link: the horizontal axis denotes the number of channels sharing a single bonded laser. The dotted line indicates the single-channel electrical power consumption of VCSEL-based multi-mode optical links. The assumptions are: 1) 10 Gb/s single-channel data rate; 2) each channel is individually encoded using a modulator with 100 fJ/bit power consumption; 3) receiver sensitivity is -18 dBm; and 4) the bonded laser has a threshold power of 30 mW and 4% slope efficiency [28].

threshold power (~ 30 mW [28]) due to less mature fabrication processes. Certainly the hybrid laser integration technology is still much less developed to date compared to VCSELs and significant improvements are thus expected by design and processing optimization. On the other hand, most VCSELs are directly modulated because of its surface emitting configuration. A VCSEL has to be pumped to high output power in order to be modulated at a high data rate of 10 Gb/s. Direct modulation of a state-of-the-art VCSEL at 10 Gb/s typically requires ~ 15 mW [29] laser power. Fig. 2 compares the single channel power consumption at 10 Gb/s for our technology and that of VCSEL-based links. Since our approach employs external modulators, using a single bonded laser for different channels will further reduce the power consumption, which largely mitigates the high threshold power issue plaguing bonded lasers. In addition, when considering the electrical circuits driving the optical devices, our approach has significant advantage in power consumption because the electroabsorption modulators (equivalent to reverse-biased diodes) used in this case requires much lower power driver circuits compared to VCSEL's driver circuits which switch at very high current levels. The overall link power consumption is thus expected to be lower in our approach than in the VCSEL approach.

Finally, we note that reach of the technology will ultimately be limited by the wafer size, since we propose to fabricate the waveguides by imprint followed by delamination from a handler substrate, and large-area (full wafer size) nanoimprint stamps are already commercially available. It is also possible to create waveguides whose lengths are not limited by the wafer size by pursuing a roll-to-roll printing approach and scale the reach of our technology even further, although it is outside the scope of our paper.

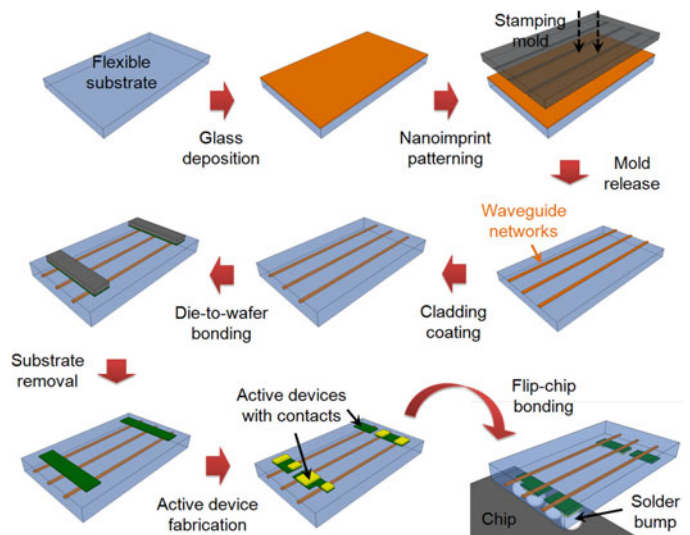


Fig. 3. Fabrication process of the flexible photonics interconnect platform

III. EXPERIMENT RESULTS AND DISCUSSIONS

A. Overview of the Flexible Photonic Interconnect Platform Fabrication Process

We choose to use chalcogenide glasses (ChGs, amorphous compounds containing S, Se or Te) as the waveguide material. Several reasons underlie our material choice:

- 1) ChGs exhibit minimal optical attenuation at the 1550 nm telecommunication wavelengths (< 1 dB/m);
- 2) these glass materials are compatible with monolithic integration on flexible substrates given their amorphous structure and low deposition temperature (substrate held at room temperature during deposition);
- 3) ChGs are amenable to large-area, roll-to-roll patterning using thermal nanoimprint [30]. In the imprint process, the glass film is directly molded to the desired shape without resorting to an additional pattern transfer step. The technique potentially allows the fabrication of photonic links whose length is not limited by semiconductor substrate size;
- 4) unlike a lot of crystalline materials which have a narrow, well-defined stoichiometric range, the glasses have almost infinite capacity for composition alloying and property fine-tuning. For example, refractive indices of the glass can be adjusted from 2–3.5 via composition tuning, and thermal stability of the materials can also be engineered to meet the Telcordia reliability standards. The high refractive indices of these glasses are critical to high-density integration as explained in the previous section.

Fig. 3 illustrates the proposed fabrication process flow of the flexible photonic link platform. The glass films are deposited using thermal evaporation, followed by thermal nanoimprint using an elastomer stamp to pattern the waveguide link networks. The elastomer stamps for imprint are fabricated following standard replica molding protocols. To minimize optical scattering loss caused by sidewall roughness, lithographically defined resist patterns used for replica molding of elastomer stamps are

treated with a thermal reflow step to remove residual surface roughness via the interaction of surface tension. Waveguides produced using the process feature a smooth surface finish with sub-nm RMS roughness and low optical loss. A thin top cladding polymer layer is subsequently spin coated on top of the waveguides following the imprint mold release step. The polymer coating also serves as an adhesive layer for III–V die bonding onto the flexible substrate. The active devices are fabricated using alignment-free “die-to-wafer” bonding, a process that has been successfully employed to demonstrated III–V heterogeneous integration on Si [16], [18]. In the last step, the flexible link is flip-chip bonded onto chips to complete the fabrication process.

B. Flexible Photonic Waveguide Fabrication and Characterization

We fabricated chalcogenide glass waveguides monolithically on polyimide (PI) plastic substrates in two composition systems: As_2Se_3 binary glass and $\text{Ge}_{23}\text{Sb}_7\text{S}_{70}$ ternary alloy. The bulk glass was prepared using a melt-quenching process. Glass thin film of ~ 400 nm thickness was deposited by thermal evaporation from bulk glasses. During deposition, the substrate was kept near room temperature (< 50 °C). More details concerning the bulk glass preparation [31] and film deposition processes may be found elsewhere [32], [33]. PI–silicone–PI tri-layer films was used as the flexible substrate material. As we show using finite element mechanical analysis in a couple of parallel publications [34], [35], the low Young’s modulus (~ 2 MPa) silicone rubber layer serves as an effective agent to relieve strain on the PI layer surfaces where the photonic devices reside during bending deformation, thus enabling superior mechanical robustness of the flexible photonic waveguide devices. To fabricate the master mold for imprint, a NR9–1000PY photoresist (Futurrex, inc.) pattern was first defined on a Si wafer using contact lithography, and then annealed at 135 °C for 5 s to reflow the NR9 polymer resist and create a smooth surface finishing. The master mold can be repeatedly used for replica molding fabrication of the PDMS soft stamp. An elastomer stamp was made by casting liquid PDMS (Sylgard 184, Dow Corning, Inc.) onto the master mold and first baked at 80 °C for 12 h and then baked at 110 °C for 5 h to fully cure the elastomer. The imprint was then performed in a N_2 purged glove box by pressing PDMS stamps against glass thin film samples under a constant pressure of 25 MPa and a temperature of 250 °C for 25 min. Finally, an SU-8 polymer (MicroChem, Inc.) layer was spin coated on the imprinted structures to protect the devices against surface degradation and serve as the adhesive bonding agent for subsequent III–V die attachment. Fig. 4(a) shows a fabricated flexible photonic waveguide sample wrapped around a rod with a radius of 5 mm.

Optical transmission characteristics of the waveguides at 1550 nm wavelength were measured using an Agilent/HP 81680A external cavity tunable laser. Paper-clip patterns with different waveguide lengths were used for loss evaluation. Fig. 4(b) shows the transmitted intensity (averaged over nine different waveguides) as a function of waveguide lengths. Prop-

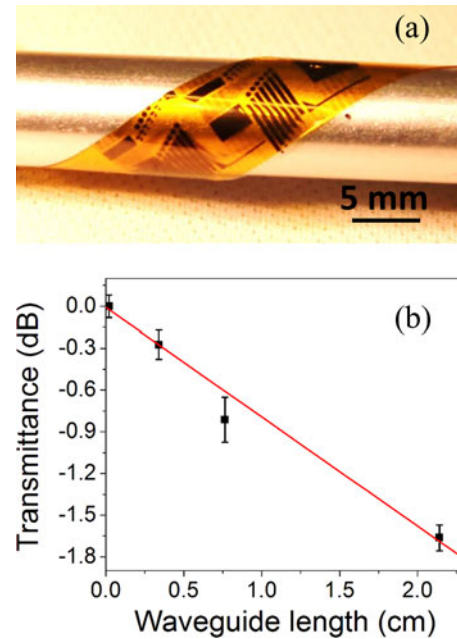


Fig. 4. (a) Photo of a flexible waveguide sample wrapped around a 5 mm diameter rod; (b) dots: measured transmitted intensity as a function of device length; slope of the fitted line yields a waveguide loss of (0.8 ± 0.3) dB/cm.

agation loss can be inferred from the slope of the curve to be (0.8 ± 0.3) dB/cm. Surface morphology of the imprinted waveguides was characterized using atomic force microscopy prior to SU-8 coating, which yielded an average surface RMS roughness of 0.7 nm. The smooth surface finish inherited from the reflow treated resist pattern contributes to the low optical loss measured in our devices: simple scattering loss estimation using the Payne–Lacey theory [36] indicates that roughness scattering accounts for < 0.1 dB/cm in the waveguide loss, and therefore, the majority of the loss contribution comes from material attenuation and discrete defects on the substrates, both of which are expected to be mitigated through further processing optimization.

According to our nano-mechanical analysis [34], the unique tri-layer substrate configuration shifts the mechanical neutral plane to the surface of the PI layer where the photonic devices are located. At the mechanical neutral plane, strain vanishes during bending deformation. Therefore, by adopting a modified “neutral plane” design paradigm [37], [38] to strategically place the photonic devices at the PI layer surface, flexible photonic links with large bending flexibility can be demonstrated. To test the mechanical reliability of our flexible photonic devices, we fabricated a series of pulley-coupled micro-disk resonators [39] on flexible substrates and tested their optical performance when the devices underwent mechanical deformation. Fig. 5 plots the resonator Q-factors and extinction ratios as functions of bending curvature, measured when the devices were bent. The test revealed no measurable optical performance degradation. We further tested the devices’ optical performance after multiple bending cycles at 0.5 mm bending radius, and little change was observed even after 100 bending cycles [34]. Optical microscope observation further revealed the absence of micro-cracks

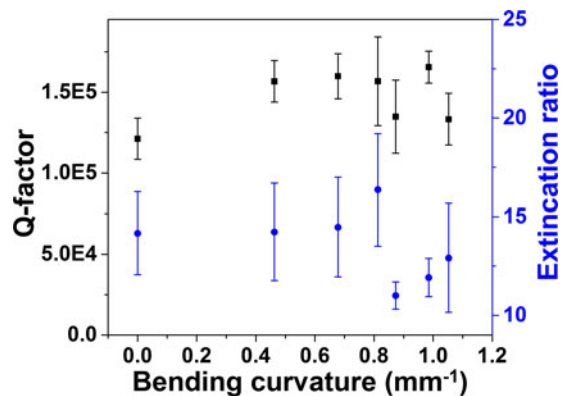


Fig. 5. Loaded Q-factors and extinction ratios of flexible micro-disk glass resonators as functions of bending curvature measured during bending.

or delamination in the layers, indicating that our devices are robust against mechanical deformation.

C. III–V Die Bonding on Flexible Substrates

We adopted an adhesive die bonding process for active component integration on flexible substrates. Since the bonding process use unpatterned III–V semiconductor die rather than fabricated III–V active devices, no alignment is required in the bonding step. The III–V die with multiple quantum well (MQW) active layers are patterned to form active components only after bonding, and alignment of the III–V devices to the glass waveguides underneath is guaranteed in the lithographic patterning process. In this paper, we will discuss our initial results on adhesive-based GaAs wafer bonding onto flexible substrates.

After glass waveguide imprint fabrication, a thin top cladding polymer layer was spin coated on top of the waveguides to serve both as a top protective cladding and as an adhesive for III–V die bonding. The key to good bonding quality is to ensure planarity of the bonding surfaces, which requires high degree of planarization (DOP) of the polymer coating. Prior reports have successfully demonstrated III–V die bonding using BCB polymers. Here we show that commercially available SU-8 epoxy can yield superior planarization results, and it also serves as an excellent bonding agent with robust mechanical and thermal characteristics ideal for heterogeneous integration on both traditional semiconductor wafers and plastic substrates.

SU-8 is an epoxy-based negative photoresist. Unexposed SU-8 behaves as a thermoplastic with a low glass transition temperature (T_g) of 50 °C [40] which can be reflowed to create an ultra-smooth surface regardless of the underlying substrate morphology. However, upon UV or thermal polymerization, SU-8 turns to a highly cross-linked, thermoset polymer ($T_g > 200$ °C) [40] with excellent chemical and mechanical stability which can withstand subsequent mechanical lapping and device processing. We exploited this unique feature of SU-8 for ultra-thin coating planarization. In our process, we first attached the flexible substrate to a rigid handler. A SU-8 layer with a thickness slightly larger than the waveguides was spin coated onto the flexible substrate, which was partially exposed under UV light after soft bake on a hotplate at 60 °C and 95 °C for 30 s,

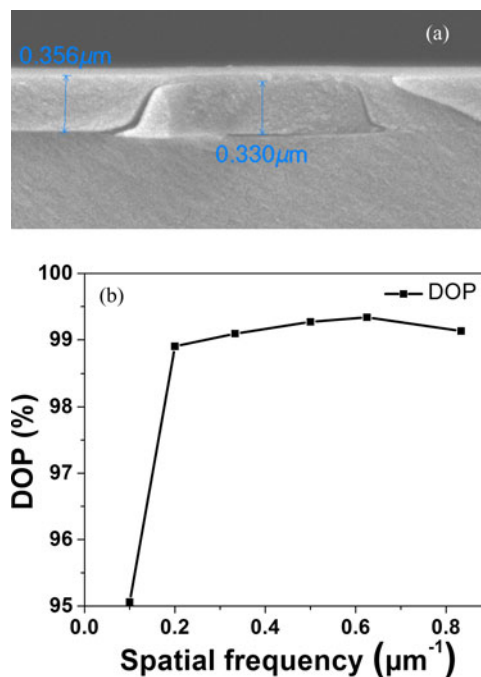


Fig. 6. (a) SEM cross-sectional image of a Ge–Sb–S glass waveguide with a planarizing SU-8 overcoating showing a high DOP of 98%; (b) ultra-thin SU-8 coating DOP as a function of spatial frequency. The SU-8 planarization process consistently yields a DOP above 95% over micron-sized features.

respectively. The soft bake step allows the SU-8 layer to reflow and planarize the surface. III–V die were then bonded to the sample using a home built pressure loading setup at 90 °C for 20 min and 150 °C for 10 min in a vacuum oven. The thermal treatment during bonding triggered thermal cross-linking of SU-8 to transform the layer into a mechanically robust adhesive between the III–V die and the flexible substrate. The III–V substrate was subsequently removed by mechanical thinning to ~ 15 μm thickness followed by chemical etching to create a semiconductor nanomembrane containing the MQW active region. It has been well established that semiconductor nanomembranes can be highly flexible despite the intrinsic rigidity of its constituent semiconductor material, making it compatible with flexible substrate integration.

Fig. 6(a) shows a cross-sectional SEM image of an ultra-thin SU-8 overcoating (30 nm in thickness) on top of a Ge–Sb–S chalcogenide glass waveguide. DOP measured from the SEM image is 98%, a record for such ultra-thin polymer planarization coatings. We further performed planarization tests on periodic glass grating patterns to extract transfer function of the planarization process. Fig. 6(b) plots the DOP as a function of spatial frequency of underlying surface features (i.e., inverse of the grating period). The DOP consistently stays above 95% for micron-sized features. Such planarization performance is considerably better than previous reports using thick SU-8, BCB, or polyimide as the planarizing agent.

Fig. 7 shows photos of a bonded, unpatterned GaAs dice before and after mechanical thinning on a polisher equipped with a custom-designed precision thickness control accessory. The SU-8 layer exhibited excellent adhesion during the mechanical

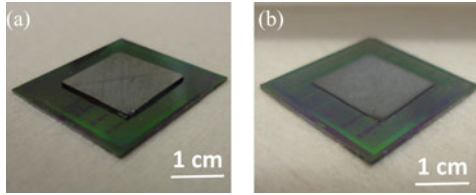


Fig. 7. Photos of a bonded GaAs dice on Ge-Sb-S waveguides (a) before and (b) after substrate thinning.

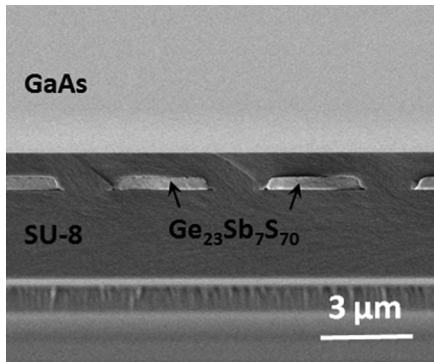


Fig. 8. SEM cross-sectional image of the bonded GaAs dice after substrate thinning, showing excellent interface adhesion free of delamination.

lapping process and no delamination was observed at the bonding interface, as is shown in the cross-sectional SEM image in Fig. 8. Future work will involve chemical thinning of the III-V substrate following mechanical lapping to create thin active MQW structures optically coupled to waveguides for a full photonic link demonstration.

IV. CONCLUSION

In this paper, we present a novel chip-to-chip interconnect technology based on a fully-integrated flexible photonics platform. Compared to current board-level optical interconnect architectures using fibers or multi-mode waveguides, our solution has the following advantages: 1) high bandwidth density scalable to 100 Tb/cm² and beyond; 2) simplified packaging process as no optical alignment is required during packaging; and 3) the mechanical flexibility of the links enables significant degrees of freedom for deployment.

We also report initial experimental results on the fabrication and characterization of the flexible photonics platform. Low loss (0.8 dB/cm), high-index-contrast chalcogenide glass waveguides were fabricated using a single-step, resistless thermal nanoimprint patterning process. Superior mechanical flexibility of the waveguide devices (sub-mm bending radius) was attained using nano-mechanical designs to minimize strain exerted on the photonic device layer during mechanical deformation. We further validated a SU-8 planarization and adhesive bonding process for III-V active photonic integration on the flexible substrates. These results pave the path towards the demonstration of a novel planar, flexible optical interconnect platform with fully-integrated optoelectronic functionalities.

REFERENCES

- [1] D. Lu, "Recent advances on chip-to-chip optical interconnect," in *Proc. Photon. Optoelectron. Meet.*, 2009, pp. 75160 O-1–75160-14.
- [2] M. D. W. BOCKSTAELE, "Chip-to-chip parallel optical interconnects over optical backpanels based on arrays of multimode waveguides," in *Proc. 9th Annu. Symp. IEEE/LEOS Benelux Chapter*, 2004, pp. 61–64.
- [3] F. E. Doany *et al.*, "Waveguide-coupled parallel optical transceiver technology for Tb/s-class chip-to-chip data transmission," in *Integr. Optoelectron. Devices*, 2008, pp. 68990 V-1–68990 V-7.
- [4] C. Kromer *et al.*, "A 100-mW 4 × 10 Gb/s transceiver in 80-nm CMOS for high-density optical interconnects," *IEEE J. Solid-State Circuits*, vol. 40, pp. 2667–2679, 2005.
- [5] M.-J. Li *et al.*, "Multicore fiber for optical interconnect applications," in *Proc. 17th Opto-Electron. Commun. Conf.*, 2012, pp. 564–565.
- [6] G. Van Steenberge *et al.*, "MT-compatible laser-ablated interconnections for optical printed circuit boards," *J. Lightw. Technol.*, vol. 22, pp. 2083–2090, 2004.
- [7] G. L. Bona *et al.*, "Characterization of parallel optical-interconnect waveguides integrated on a printed circuit board," in *Proc. SPIE*, 2004, vol. 5453, pp. 134–141.
- [8] A. V. Krishnamoorthy, R. Ho, X. Zheng, H. Schwetman, J. Lexau, P. Koka, L. Guoliang, I. Shubin, and J. E. Cunningham, "Computer systems based on silicon photonic interconnects," *Proc. IEEE*, vol. 97, no. 7, pp. 1337–1361, Jul. 2009.
- [9] C. Batten, A. Joshi, J. Orcutt, A. Khilo, B. Moss, C. W. Holzwarth, M. A. Popovic, L. Hanqing, I. H. Smith, J. L. Hoyt, F. X. Kartner, R. J. Ram, V. Stojanovic, and K. Asanovic, "Building many-core processor-to-DRAM networks with monolithic CMOS silicon photonics," *IEEE Micro*, vol. 29, no. 4, pp. 8–21, Jul./Aug. 2009.
- [10] R. T. Chen, L. Lin, C. Choi, Y. J. Liu, B. Bihari, L. Wu, S. Tang, R. Wickman, B. Picor, M. K. Hibb-Brenner, J. Bristow, and Y. S. Liu, "Fully embedded board-level guided-wave optoelectronic interconnects," *Proc. IEEE*, vol. 88, no. 6, pp. 780–793, Jun. 2000.
- [11] Y. Liu, L. Lin, C. Choi, B. Bihari, and R. T. Chen, "Optoelectronic integration of polymer waveguide array and metal-semiconductor-metal photodetector through micromirror couplers," *IEEE Photon. Technol. Lett.*, vol. 13, no. 4, pp. 355–357, Apr. 2001.
- [12] M. Haney *et al.*, "Chip-scale integrated optical interconnects: A key enabler for future high-performance computing," in *Proc. SPIE*, 2012, vol. 8267, pp. 82670-X-1–82670-X-12.
- [13] R. Nair *et al.*, "Hybrid chip-scale optical interconnects using multiple quantum well devices bonded to silicon," in *Proc. IEEE Opt. Interconnects Conf.*, 2012, pp. 18–19.
- [14] T. Gu, *et al.*, "Chip-level multiple quantum well modulator-based optical interconnects," *J. Lightwave Technol.*, in press.
- [15] T. Gu, R. Nair, and M. W. Haney, "Prismatic coupling structure for intra-chip global communication," *IEEE J. Quantum Electron.*, vol. 45, no. 4, pp. 388–395, Apr. 2009.
- [16] D. Liang *et al.*, "Hybrid integrated platforms for silicon photonics," *Materials*, vol. 3, pp. 1782–1802, 2010.
- [17] G. Roelkens *et al.*, "Adhesive bonding of InP/InGaAsP dies to processed silicon-on-insulator wafers using DVS-bis-benzocyclobutene," *J. Electrochemical Soc.*, vol. 153, pp. G1015–G1019, 2006.
- [18] G. Roelkens *et al.*, "III-V/Si photonics by die-to-wafer bonding," *Mater. Today*, vol. 10, pp. 36–43, 2007.
- [19] L. Schares, J. A. Kash, F. E. Doany, C. L. Schow, C. Schuster, D. M. Kuchta, P. K. Pepeljugoski, J. M. Trehwella, C. W. Baks, R. A. John, L. Shan, Y. H. Kwark, R. A. Budd, P. Chiniwalla, F. R. Libsch, J. Rosner, C. K. Tsang, G. S. Patel, J. D. Schaub, R. Dangel, F. Horst, B. J. Offrein, D. Kucharski, D. Guckenberger, S. Hegde, H. Nyikal, L. Chao-Kun, A. Tandon, G. R. Trott, M. Nystrom, D. P. Bour, M. R. T. Tan, and D. W. Dolfi, "Terabus: Terabit/second-class card-level optical interconnect technologies," *IEEE J. Sel. Topics Quantum Electron.*, vol. 12, no. 5, pp. 1032–1044, Sep./Oct. 2006.
- [20] E. Bosman *et al.*, "Flexible embedded active optical link," *Proc. SPIE*, vol. 6992, pp. 69920 V-1–69920 V-10, 2008.
- [21] T. Shibata and A. Takahashi, "Flexible opto-electronic circuit board for in-device interconnection," in *Proc. 58th Electron. Compon. Technol. Conf.*, 2008, pp. 261–267.
- [22] H. Gan, *et al.*, "Pb-free microjoints (50/spl mu/m pitch) for the next generation microsystems: The fabrication, assembly and characterization," presented at the 56th Electronic Components and Technology Conf., San Diego, CA, USA, 2006, p. 6.
- [23] I. A. Young, E. Mohammed, J. T. S. Liao, A. M. Kern, S. Palermo, B. A. Block, M. R. Reshotko, and P. L. D. Chang, "Optical I/O

- technology for tera-scale computing," *IEEE J. Solid-State Circuits*, vol. 45, no. 1, pp. 235–248, Jan. 2010.
- [24] J. Hofrichter *et al.*, "A low-power high-speed InP microdisk modulator heterogeneously integrated on a SOI waveguide," *Opt. Exp.*, vol. 20, pp. 9363–9370, 2012.
- [25] D. Ahn *et al.*, "High performance, waveguide integrated Ge photodetectors," *Opt. Exp.*, vol. 15, pp. 3916–3921, 2007.
- [26] S. J. Madden *et al.*, "Long, low loss etched As₂S₃ chalcogenide waveguides for all-optical signal regeneration," *Opt. Exp.*, vol. 15, pp. 14414–14421, 2007. (Assuming 0.1 dB/cm waveguide propagation loss and 40 cm link length. Note that chalcogenide glass waveguides with propagation loss as low as 0.05 dB/cm have been experimentally demonstrated.)
- [27] WTD. 2009, *10Gb/s PIN-TIA ROSA PTCM992-405*. [Online]. Available: <http://www.wtd.com.cn/en/uploadfile/ptcm992-405.pdf>
- [28] M. Lamponi, S. Keyvaninia, C. Jany, F. Poingt, F. Lelarge, G. de Valicourt, G. Roelkens, D. Van Thourhout, S. Messaoudene, J.-M. Fedeli, and G.H. Duan, "Low-threshold heterogeneously integrated InP/SOI lasers with a double adiabatic taper coupler," *IEEE Photon. Technol. Lett.*, vol. 24, no. 1, pp. 76–78, Jan. 2012.
- [29] JDSU. 2012. *JDSU 850 nm 10 G connectorized transmit optical sub-assembly (TOSA)*. [Online]. Available: <http://www.jdsu.com/ProductLiterature/pl-xxd-00-s40-cx-ds-oc-ae.pdf>
- [30] Y. Zou, *et al.*, "High-Performance, High-Index-Contrast Chalcogenide Glass Photonics on Silicon and Unconventional Non-planar Substrates," arXiv:1308.2749. Available: <http://arxiv.org/abs/1308.2749>.
- [31] L. Petit *et al.*, "Correlation between physical, optical and structural properties of sulfide glasses in the system Ge–Sb–S," *Mater. Chem. Phys.*, vol. 97, pp. 64–70, 2006.
- [32] J. J. Hu *et al.*, "Fabrication and testing of planar chalcogenide waveguide integrated microfluidic sensor," *Opt. Exp.*, vol. 15, pp. 2307–2314, Mar. 5, 2007.
- [33] H. Lin *et al.*, "Demonstration of high-Q mid-infrared chalcogenide glass-on-silicon resonators," *Opt. Lett.*, vol. 38, pp. 1470–1472, 2013.
- [34] L. Li, *et al.*, "3-D integrated flexible glass photonics," arXiv:1307.5937v2. Available: <http://arxiv.org/abs/1307.5937v2>.
- [35] J. Hu *et al.*, "Flexible integrated photonics: Where materials, mechanics and optics meet [Invited]," *Opt. Mater. Exp.*, vol. 3, pp. 1313–1331, 2013.
- [36] J. Lacey and F. Payne, "Radiation loss from planar waveguides with random wall imperfections," *IEE Proc. J. Optoelectron.*, vol. 137, no. 4, pp. 282–288, Aug. 1990.
- [37] D.-H. Kim *et al.*, "Stretchable and foldable silicon integrated circuits," *Science*, vol. 320, pp. 507–511, 2008.
- [38] D.-H. Kim *et al.*, "Materials for stretchable electronics in bioinspired and biointegrated devices," *MRS Bull.*, vol. 37, pp. 226–235, 2012.
- [39] J. Hu *et al.*, "Planar waveguide-coupled, high-index-contrast, high-Q resonators in chalcogenide glass for sensing," *Opt. Lett.*, vol. 33, pp. 2500–2502, 2008.
- [40] Y. Zhang *et al.*, "Fabrication of hierarchical pillar arrays from thermoplastic and photosensitive SU-8," *Small*, vol. 6, pp. 768–775, 2010.

Authors' biographies not available at the time of publication.